I J C R M
International Journal of Contemporary Research In Multidisciplinary

Research Article

Computational QSAR Analysis of New Thiazol Derivatives as Inhibitors

Ashok Nagore[1*], **Sunita Gupta** [2]
[1-2] Department of Chemistry, PMCOE, Govt. Science College, Rewa, Madhya Pradesh, India

Corresponding Author: *Ashok Nagore

DOI: https://doi.org/10.5281/zenodo.19697004

Abstract

In order to support the development of new 11β-hydroxysteroid dehydrogenase type 1 (11β-HSD1) inhibitors based on the pseudothiohydantoin scaffold and perhaps provide innovative treatments for metabolic illnesses, this research attempts to create a predictive model. 56 derivatives of 2-aminothiazol-4(5h)-one, for which the 11β-HSD1 inhibitory action was previously described, were subjected to the Quantitative Structure–Action Relationship (QSAR) study. Dragon software was utilised to compute the molecular descriptors, and Gaussian software was utilised for geometry optimisation. Regression analysis between the top ten preselected descriptors and the activity of the examined analogues was conducted using an Artificial Neural Network (ANN) technique. Using a network architecture 10-11-1 and a Broyden–Fletcher–Goldfarb–Shanno learning algorithm, a predictive model was created. Cross-validation and y-randomisation techniques bolstered the model's dependability. With a determination coefficient (R2) of 0.9482, the model demonstrated great accuracy, and internal validation verified its validity with a cross-validated R2 (Q2) of 0.9944. The QSAR model was created using four sets of topological indices (GALVEZ, 2D autocorrelations, 2D matrix-based descriptors, and Burden eigenvalues) and three classes of 3D descriptors (GETAWAY, 3D-MoRSE, and RDF descriptors). Compounds with cyclohexyl and 2-(tetrahydro-2H-pyran-2-yl)methyl residues substituted at the amino group and different substituents at C-5 of the thiazole ring may be viable candidates for future chemical synthesis and biological evaluation, according to the developed model, which was used to predict the 11β-HSD1 inhibitory activity of four designed series of 2-aminothiazol-4(5h)-one derivatives.

Manuscript Information

- **ISSN No:** 2583-7397
- **Received:** 14-03-2026
- **Accepted:** 10-04 2026
- **Published:** 22-04-2026
- **IJCRM:**5(2); 2026: 742-755

- **Plagiarism Checked:** Yes
- **Peer Review Process:** Yes

How to Cite this Article

Nagore A, Gupta S. Computational QSAR Analysis of New Thiazol Derivatives as Inhibitors. Int J Contemp Res Multidiscip. 2026;5(2):742-755.

Access this Article Online

www.multiarticlesjournal.com

KEYWORDS: Quantitative structure–activity relationship (QSAR); 11β-hydroxysteroid dehydrogenase type 1 (11β-HSD1) inhibitors; Metabolic diseases; Artificial neural networks (ANNs)

1. INTRODUCTION

11β-Hydroxysteroid dehydrogenase type 1 (11β-HSD1) is a crucial enzyme in the metabolism of glucocorticoids, which are vital hormones regulating energy metabolism, immune and inflammatory responses, and the body's reaction to stress [1]. This NADPH-dependent oxidoreductase catalyses the conversion of inactive cortisone into active cortisol [2]. Alongside 11β-hydroxysteroid dehydrogenase type 2, it plays a role in managing the body's cortisol levels.

11β-HSD1 is present in numerous tissues, with particularly high levels found in the liver, adipose tissue, central nervous system (CNS), skeletal muscle, pancreatic islets, immune cells, and gonads [3, 4]. Its activity in the liver is significant for gluconeogenesis, while in adipose tissue, it impacts adipogenesis and lipolysis [5, 6]. Dysregulation of 11β-HSD1 in these two tissues is linked to metabolic syndrome (MetS) [5]. MetS is a condition defined by a cluster of issues, such as central obesity, high blood pressure, type 2 diabetes, abnormal blood lipid levels, and insulin resistance [7].

Studies on transgenic mice overexpressing 11β-HSD1 in adipose tissue revealed characteristic signs of metabolic syndrome, including obesity, insulin resistance, hypertension, and dyslipidemia [4]. Excessive 11β-HSD1 activity specifically influences visceral fat, as demonstrated in animal studies [8, 9]. Elevated 11β-HSD1 activity results in higher cortisol levels. Cortisol, in turn, directly influences lipoprotein lipase, an enzyme that breaks down circulating triacylglycerol (TAG) into free fatty acids and glycerol [10]. This increased supply of free fatty acids promotes their uptake and storage, particularly in the visceral region. Furthermore, prolonged high cortisol levels impact adipocyte differentiation, leading to more mature adipocytes and significant hypertrophy [10]. Evidence for this comes from transgenic mouse models overexpressing 11β-HSD1 in adipose tissue, which exhibited visceral obesity (characterised by enlarged adipocytes), insulin resistance, hyperlipidemia, and hypertension [9]. Likewise, liver-specific overexpression boosts gluconeogenesis and contributes to insulin resistance [11]. Increased 11β-HSD1 expression in the liver has also been observed in patients with hypertension linked to cortisol-driven angiotensinogen upregulation [12]. Mice genetically engineered for excessive hepatic 11β-HSD1 expression developed hypertension and a mild form of insulin resistance [13].

Inhibition of 11β-HSD1 is currently a prospective target in the treatment of metabolic illnesses because of the crucial role that 11β-HSD1 plays in the pathophysiology of metabolic syndrome. According to scientific studies, when type 2 diabetics use 11β-HSD1 inhibitors, their blood sugar levels drop, resulting in a decrease in body weight and insulin resistance [14]. A notable advancement of selective 11β-HSD1 inhibitors was seen in the first two decades of the twenty-first century. Several substances, such as BVT-3498, AMG-221, or PF-915275, had the chance to be examined in the initial stages of clinical studies. Nevertheless, the research was discontinued due to the disappointing results [15-17]. Therefore, more investigation and refinement are required to create a class of strong and specific 11β-HSD1 inhibitors, since the current class of medications still holds promise and could offer a fresh approach to treating metabolic disorders.

A class of drugs with a 2-aminothiazol-4(5H)-one (pseudothiohydantoin) group in their structure served as the basis for earlier research on the quest for selective 11β-hydroxysteroid dehydrogenase type 1 inhibitors. Recent research has produced six series of 2-aminothiazol-4(5H)-one derivatives (each comprising nine or ten compounds) with different substituents at C-5 of the thiazole ring, including allyl groups at the amino group [18], methyl groups [19], isopropyl groups [20], tert-butyl groups [21], adamantly [22], and cyclopentyl [23] (Fig. 1). Every series was examined for 11β-hydroxysteroid dehydrogenase type 1 inhibition. Every series was examined for 11β-hydroxysteroid dehydrogenase type 1 inhibition. In order to create a mathematical model that may direct the creation of structurally advantageous 2-aminothiazol-4(5H)-one analogues, the current work was carried out using 56 pseudothiohydantoin derivatives. Computational models that might speed up the discovery and screening of more potent candidates are desperately needed, given the poor performance of earlier inhibitors in clinical trials. This problem is solved by the current QSAR method, which accurately predicts 11β-HSD1 inhibitory action.

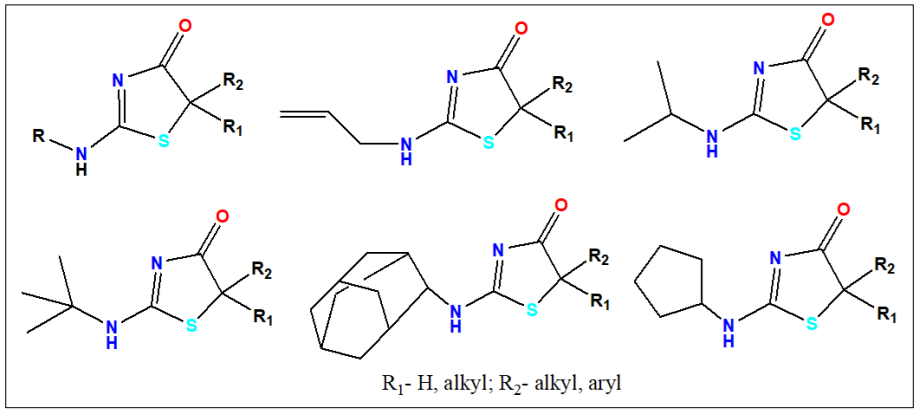

Fig. 1 Structures of synthesized 2-aminothiazol-4(5H)-one derivatives 11β-HSD1 inhibitors

2. MATERIALS AND METHODS

Energy optimization of 2-aminothiazol-4(5H)-one derivatives

Previously published experimental research on the synthesis and *in vitro* evaluation of 11β-HSD1 inhibitors provided the dataset of 2-aminothiazol-4(5H)-one derivatives employed in this investigation [18–23]. Gaussian 16 (Gaussian Inc., Wallingford, CT, USA) was used for all quantum-mechanical computations for the 56 investigated 2-aminothiazol-4(5H)-one derivatives (Table 1) [24]. Compound models were first created using GaussView 6 (Gaussian Inc., Wallingford, CT, USA) [25]. The B3LYP functional was then used to optimise the models using the 6–311++G(d,p) basis set [26-30]. Frequency computations at the same theoretical level verified the nature of the stationary points and ensured that there were no imaginary frequencies in the optimised structures.

Table 1: Chemical structures of the studied 2-aminothiazol-4(5H)-one derivatives possessing 11β-HSD1 inhibitory activity

Compound	R	R_1	R_2	% of 11β-HSD1 inhibition 10 μM [18–23]	log $I_{11β\text{-}HSD1}$
1a	CH_2=CH-CH_2-	H	H	0	0
1b		H	CH_3	0	0
1c		H	C_2H_5	0	0
1d		H	*n*-C_3H_7	0	0
1e		H	$CH(CH_3)_2$	0	0
1f		CH_3	CH_3	0	0
1g		H	C_6H_5	0	0
1h		H	*p*-BrC_6H_4	13.46	1.16
1i		C_5H_{10cycl}		71.27	1.86
1j		C_3H_{6cycl}		38.03	1.59
2b	CH_3-	H	CH_3	0	0.00
2c		H	C_2H_5	0	0.00
2d		H	*n*-C_3H_7	0	0.00
2e		H	$CH(CH_3)_2$	21.13	1.34
2f		CH_3	CH_3	22.25	1.37
2g		H	C_6H_5	0	0.00
2h		H	*p*-BrC_6H_4	17.00	1.26
2i		C_5H_{10cycl}		48.00	1.69
2j		C_3H_{6cycl}		23.00	1.38
3b	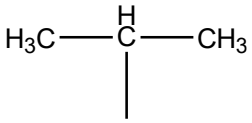	H	CH_3	0	0.00
3c		H	C_2H_5	0	0.00
3d		H	*n*-C_3H_7	0	0.00
3e		H	$CH(CH_3)_2$	18.86	1.30
3f		CH_3	CH_3	18.06	1.28
3g		H	C_6H_5	0	0.00
3h		H	*p*-BrC_6H_4	27.58	1.46
3i		C_5H_{10cycl}		54.53	1.74
3j		C_3H_{6cycl}		20.94	1.34
4b	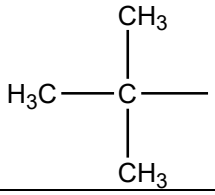	H	CH_3	16.29	1.24
4c		H	C_2H_5	20.11	1.32
4d		H	*n*-C_3H_7	29.17	1.48
4e		H	$CH(CH_3)_2$	44.27	1.66
4f		CH_3	CH_3	29.70	1.49
4g		H	C_6H_5	26.85	1.44
4h		H	*p*-BrC_6H_4	10.31	1.05
4i		C_5H_{10cycl}		82.54	1.92
4j		C_3H_{6cycl}		23.61	1.39
5a	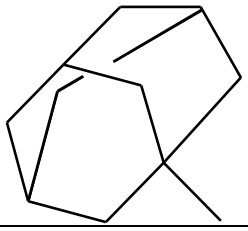	H	H	22.27	1.37
5b		H	CH_3	62 .1 5	1. 80
5c		H	C_2H_5	6 9. 2 2	1. 85
5d		H	*n*-C_3H_7	7 2. 3 7	1.87
5e		H	$CH(CH_3)_2$	7 6 .40	1 .89
5f		CH_3	CH_3	65 . 99	1. 83
5g		H	C_6H_5	46 3 2	1 .68
5h		H	*p*-BrC_6H_4	15.30	1.21
5i		$C_5H_{10c\ ycl}$		8 2. 82	1.92
5j		C_3H_{6cycl}		74.13	1. 88
6b		H	CH_3	10 .9 4	1. 08
6c		H	C_2H_5	21. 33	1. 3 5
6d		H	*n*- C_3H_7	56 .58	1 .76
6e		H	$CH(CH_3)_2$	8 2 .93	1 .92
6f		CH_3	CH_3	53 .17	1 .73

6g	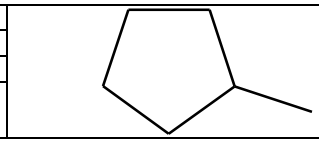	H	C_6H_5	6 . 2 9	1. 81
6h		H	*p* -Br_6H_4	86.96	1 .94
6i		C_5H_{10cycl}		90 .49	1 .96
6j		C_3H_{6cycl}		71.25	1.86

Molecular descriptors

In order to give mathematical representations of a molecule's chemical information for QSAR modelling, 5,270 molecular descriptors were obtained from DFT calculations and Dragon 7.0 (Talete, Milano, Italy) software [31, 32]. These descriptors include 0D constitutional, 1D structural, 2D topological and 3D geometrical descriptors. They are divided into 30 logical blocks. The obtained descriptors were reduced to 921 molecular parameters after objective feature selection by removing variables with zero or missing values, constant or nearly constant values, parameters with a standard deviation less than 0.0001, and highly correlated parameters (|r|> 0.95).

Regression analysis

Statistica 14.1.0.4 software (TIBCO Software Inc., Palo Alto, CA, USA) was used for the statistical study. Before doing QSAR modelling, the logarithm of the percentage of 11β-HSD1 inhibition was computed. The distribution of dependent variables was examined for possible outliers, but none were discovered in the data. The ten most significant descriptors that were appropriate for modelling were then selected using the Statistica Random Forest methods (Fig. 2 and Table 2). This was done in order to improve the prediction performance, avoid overfitting, and simplify the regression model [33]. Before ANN modelling, all molecular descriptors were scaled using min–max normalization to the range [0,1].

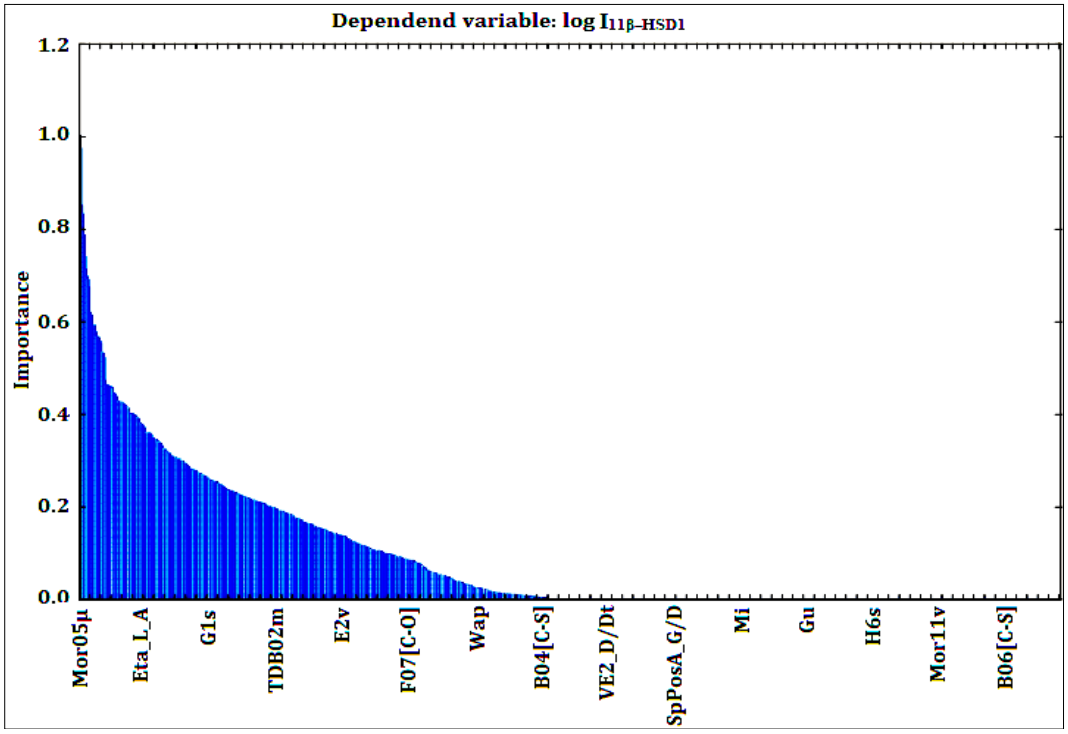

Fig 2: Descriptor importance plot

Table 2: Molecular descriptors used to train ANN models

Symbol	Variable rank	Importance
Mor05µ	100	1.000000
MATS1s	98	0.975098
R3v+	85	0.850106
R2s	83	0.832084
GGI2	79	0.787630
RDF030µ	74	0.740510
SpMin8_Bh(m)	71	0.712326
SpPosA_B(m)	70	0.697505
VE2_B(p)	69	0.691941
VE_D/Dt	67	0.673839

The next step involved using post-processing methods called STATISTICA Automated Neural Networks (SANN) to find relationships between chemical descriptors that characterise the characteristics of compounds and their 11β-HSD1-inhibitory activity. The network's output is qualitative and expressed as the logarithm of the proportion of 11β-HSD1 inhibition since the established model solves the regression problem.

For learning, cross-evaluation of network quality, and control of the learning algorithm's influence, the Statistica ANS module automatically divides the examined derivatives into training, a test, and a validation sample in a 70:15:15 ratio. The molecular

descriptors are entered into the appropriate input units during the network training process, and then the hidden and output layer units are executed one after the other. The outputs of the units in the preceding layer are added together and weighted based on their significance to get each unit's activation value. The activation function then uses it to produce the neuron's output. After the network's execution is finished, the neuron or neurons of the output layer are assigned to the intended response (in this case, 11β-HSD1-inhibitory activity) [33, 34]. Scaling input and target variables was made possible by the software's ANS module. It made it possible to create several networks with variable activation, error, and complexity functions.

Hyperparameters like network size and training algorithm control parameters can be defined by users. To lessen overfitting, dropout regularisation and early halting were used, and a hold-out test set was kept. Important neural network types, such as multilayer perceptrons, radial basis function networks, and Kohonen self-organising feature maps, are compatible with the SANN architecture. The most successful networks were displayed after the networks were trained, making it possible to choose the best-performing network without the need for a laborious trial-and-error process [34]. STATISTICA's Automated Network Search was used to optimise the network architecture by testing several topologies. Based on performance metrics on training, test, and validation datasets, the best network (10-11-1) was chosen. Training cycles, the activation function (exponential), and the learning method (BGFS) were among the hyperparameters that were automatically optimised. The ANN model used an 11-neuron hidden layer that was tuned via early halting and dropout (0.2). A sensitivity analysis was used to determine the variables' importance for the QSAR model. In the end, the model was used to predict the 11β-HSD1-inhibitory activity of 39 newly created 2-aminothiazol-4(5H)-one analogues, designated as 7b-10j.

3. RESULTS AND DISCUSSION

The structure-activity relationship of fifty-six 2-aminothiazol-4(5H)-one derivatives as 11β-HSD1 inhibitors was investigated using QSAR analysis. Gauss View 6 was used to construct 3D representations of each structure, and the Gaussian 16 software's DFT algorithm b3lyp/6–311 ++g(d,p) was used for optimisation. Fig. 3 shows examples of three-dimensional molecular formations with specific geometry.

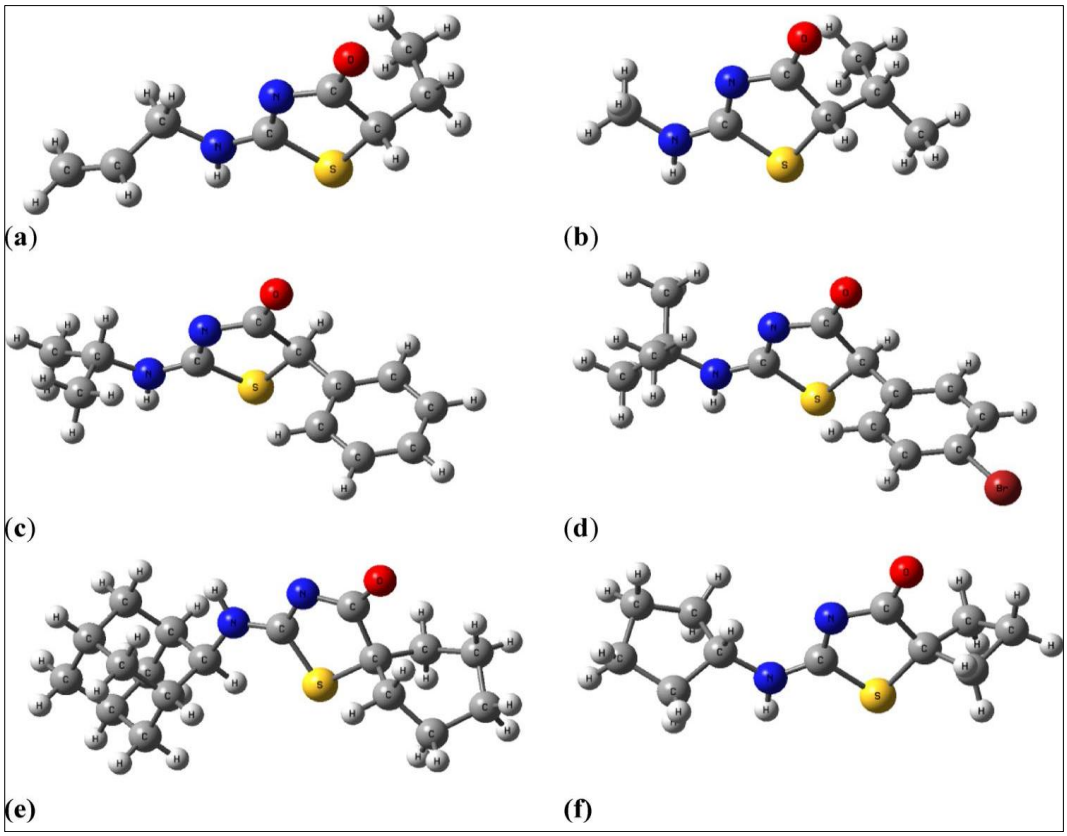

Fig 3: Geometrically optimized structures of selected 2-aminothiazol-4(5H)-one analogs: **a** 1c; **b** 2e; **c** 3g; **d** 4h; **e** 5i; **f** 6j

Dragon Software computed more than 5000 molecular descriptors for geometrically optimised structures during the molecular modelling study. From a vast pool of candidates, the top ten descriptors were chosen to enhance the predictive performance of QSAR models.

Galvez topological charge indices, 2D autocorrelations, 2D matrix-based descriptors, GETAWAY descriptors, Burden eigenvalues, 3D-MoRSE descriptors, and RDF descriptors were among the descriptor blocks that included the chosen descriptors (Tables 3 and 4). The 11β-HSD1 inhibitory activity of the investigated and 39 newly created compounds was then predicted by using these characteristics as independent variables to construct several models using artificial neural networks as a post-processing tool.

Table 3: Values of molecular descriptors selected for model building for the investigated 2-aminothiazol-4(5H)-one derivatives

Compound	Sample	Descriptors									
		Mor05u	MATS1s	R3v+	R2s	GGI2	RDF030u	SPMin8_Bh(m)	SpP0sA_Bh(m)	VE2_B(p)	VE1_D/Dt
1a	Train	-1.968	-0.084	0.062	5.636	0.667	3.243	0.000	1.512	0.264	2.704
1b	Train	− 2.439	− 0.092	0.052	5.474	1.111	6.356	0.000	1.482	0.246	2.807
1c	Train	− 2.81	− 0.067	0.047	5.266	1.111	8.778	0.403	1.463	0.23	2.961
1d	Train	− 3.487	− 0.051	0.045	5.281	1.111	10.062	0.466	1.446	0.214	3.16
1e	Train	− 3.295	− 0.078	0.033	4.844	1.333	9.841	0.434	1.456	0.219	3.125
1f	Test	− 3.051	− 0.108	0.043	4.903	1.778	8.762	0.223	1.464	0.23	2.866
1g	Test	− 2.587	− 0.083	0.052	5.992	1.333	5.301	0.488	1.455	0.215	3.044
1h	Validation	− 2.478	− 0.09	0.052	6.129	1.778	7.611	0.482	1.765	0.204	3.38
1i	Train	− 3.736	− 0.014	0.026	4.498	1.778	17.303	0.721	1.413	0.202	3.088
1j	Train	− 3.425	− 0.033	0.037	4.65	1.556	13.332	0.427	1.464	0.226	2.858
2b	Validation	− 2.108	− 0.064	0.053	5.296	1.111	4.283	0.000	1.495	0.285	2.697
2c	Train	− 2.32	− 0.04	0.051	5.447	1.111	6.827	0.000	1.475	0.262	2.822
2d	Train	− 2.924	− 0.025	0.047	5.454	1.111	8.279	0.000	1.453	0.241	2.866
2e	Train	− 2.958	− 0.054	0.036	5.057	1.333	7.982	0.000	1.464	0.248	2.926
2f	Test	− 2.54	− 0.084	0.044	4.801	1.778	6.275	0.000	1.481	0.266	2.841
2g	Test	− 2.422	− 0.058	0.055	5.919	1.333	3.828	0.381	1.462	0.242	2.951
2h	Train	− 2.297	− 0.064	0.055	6.059	1.778	5.841	0.381	1.813	0.229	3.336
2i	Train	− 3.153	0.01	0.028	4.955	1.778	16.037	0.624	1.413	0.226	2.925
2j	Train	− 3.261	− 0.005	0.039	4.978	1.556	12.073	0.000	1.476	0.26	2.738
3b	Train	− 3.072	− 0.075	0.037	5.469	1.111	7.167	0.000	1.47	0.25	2.848
3c	Train	− 3.483	− 0.059	0.043	4.797	1.111	11.555	0.370	1.448	0.234	3.001
3d	Train	− 3.34	− 0.049	0.037	4.829	1.111	11.908	0.583	1.435	0.218	3.175
3e	Validation	− 4.134	− 0.074	0.029	4.51	1.333	12.56	0.468	1.443	0.223	3.148
3f	Validation	− 3.776	− 0.096	0.037	4.56	1.778	11.551	0.215	1.451	0.234	2.921
3g	Train	− 3.716	− 0.068	0.041	5.499	1.333	8.078	0.630	1.445	0.217	2.987
3h	Validation	− 2.785	− 0.073	0.04	5.23	1.778	9.349	0.611	1.756	0.206	3.337
3i	Train	− 4.776	− 0.02	0.023	4.247	1.778	20.1	0.785	1.404	0.204	3.017
3j	Test	− 4.139	− 0.032	0.032	4.348	1.556	16.081	0.466	1.451	0.229	2.892
4b	Validation	− 3.485	− 0.098	0.032	4.38	1.333	7.685	0.000	1.457	0.248	2.98
4c	Train	− 3.646	− 0.083	0.035	4.516	1.333	10.047	0.498	1.438	0.233	3.106
4d	Validation	− 4.195	− 0.073	0.029	4.581	1.333	11.435	0.727	1.426	0.218	3.294
4e	Train	− 4.442	− 0.096	0.025	4.352	1.556	11.148	0.617	1.434	0.221	3.269
4f	Train	− 3.823	− 0.118	0.029	4.157	2.000	10.146	0.248	1.44	0.232	3.025
4g	Train	− 3.921	− 0.089	0.029	4.842	1.556	6.750	0.906	1.437	0.212	3.006
4h	Train	− 3.758	− 0.095	0.032	4.965	2.000	8.877	0.786	1.731	0.2	3.338
4i	Train	− 5.29	− 0.044	0.021	4.061	2.000	18.613	0.809	1.398	0.202	3.073
4j	Train	− 4.654	− 0.057	0.025	4.015	1.778	14.667	0.694	1.442	0.224	3.031
5a	Train	− 4.833	0.036	0.023	5.268	1.111	14.08	0.899	1.415	0.228	3.542
5b	Test	− 5.499	0.018	0.027	4.744	1.556	17.706	1.051	1.403	0.216	3.749
5c	Train	− 5.778	0.022	0.026	4.497	1.556	20.236	1.079	1.394	0.206	3.885
5d	Train	− 6.719	0.023	0.018	4.962	1.556	20.889	1.079	1.387	0.197	3.991
5e	Train	− 6.36	0.005	0.019	4.373	1.778	21.212	1.18	1.393	0.198	3.988
5f	Train	− 6.08	− 0.004	0.023	4.409	2.222	20.041	1.079	1.394	0.201	3.888
5g	Validation	− 5.89	0.032	0.024	4.98	1.778	16.544	1.181	1.4	0.174	4.28
5h	Train	− 5.675	0.03	0.029	5.084	2.222	18.804	1.181	1.622	0.16	4.294
5i	Train	− 6.559	0.035	0.019	4.624	2.222	28.349	1.232	1.37	0.181	4.237
5j	Train	− 6.707	0.034	0.021	4.637	2.000	24.203	1.079	1.398	0.19	4.05
6b	Train	− 3.424	− 0.003	0.033	5.248	1.111	13.119	0.551	1.447	0.214	3.185
6c	Train	− 3.59	0.004	0.04	4.674	1.111	15.545	0.72	1.431	0.202	3.267
6d	Train	− 4.384	0.008	0.034	4.706	1.111	16.909	0.782	1.42	0.19	3.322
6e	Train	− 4.147	− 0.013	0.029	4.493	1.333	16.624	0.772	1.427	0.195	3.334
6f	Train	− 3.857	− 0.027	0.034	4.475	1.778	15.573	0.695	1.432	0.202	3.288
6g	Test	− 3.675	0.004	0.036	5.321	1.333	12.253	0.883	1.431	0.193	3.648
6h	Train	− 3.557	0.001	0.033	5.763	1.778	15.331	0.822	1.71	0.184	3.641
6i	Train	− 4.853	0.027	0.022	4.203	1.778	24.047	0.868	1.394	0.181	3.63
6j	Train	− 4.608	0.023	0.029	4.27	1.556	20.197	0.773	1.434	0.2	3.463

About 500 neural networks with different features were trained using the Automated Network Search (ANS) algorithm. A multilayer perceptron (MLP) 10-11-1 network with the ID 344 was selected as the optimal model for depicting the relationships between after assessing the training, test, and validation performances, including correlation coefficient and sum of squares error. particular characteristics and 11β-HSD1-inhibitory activity, tackling the regression issue in question. Numerous distinct network creation involved the use of algorithms and activation functions. A Broyden-Fletcher-Goldfarb-Shanno (BFGS) learning method and exponential functions for the hidden and output layers were employed in the predictive network. Ten artificial neurons make up the input layer of the network, eleven artificial neurons make up the hidden layer, and one neuron makes up the output layer. The best-performing artificial neural network used in this study has an architecture known as the "10-11-1 model," which consists of 10 input neurons, 11 hidden layer neurons, and a single output neuron that represents expected activity.

A strong correlation between the experimental logarithm of the percentage of 11β-HSD1 inhibition (log I11β-HSD1) value and the value predicted by the network characterises the predictive QSAR MLP 10-11-1 model. For training, the correlation coefficient is 0.99; for the test set, it is 0.95; and for validation, it is 0.93. For the training, test, and validation samples, the sum of squares error between observed and predicted values was 0.002, 0.03 and 0.06, respectively. The MLP 10-11-1 model may be used to predict the 11β-HSD1 inhibitory action of new drugs based on a pseudothiohydantoin scaffold, according to the validation process published by Roy *et al*. [35]. The most used quality criteria for evaluating the accuracy and dependability of QSAR model predictions [36] are presented in Table 5.

Table 2: Selected validation parameters of the predictive MPL10-11-1 model

Parameter [35]	Value	Threshold [35]	Meaning [35]
$R^2 = 1 - \frac{\sum(Y_{obs} - Y_{cal})^2}{\sum(Y_{obs} - \bar{Y}_{training})^2}$	0.9482	~ 1 (1 means perfect correlation)	Measures the variation of observed data from the predicted one
$Q^2(or\ Q^2_{LOO}) = 1 - \frac{\sum(Y_{obs(training)} - Y_{pred(training)})^2}{\sum(Y_{obs(training)} - \bar{Y}_{training})^2}$	0.9944	> = 0.5	Cross-validated R^2 (Q^2) checked for internal validation
$PRESS = \sum(Y_{obs} - Y_{pred})^2$	1.5649		Evaluates the model using the predicted residual sum of squares
$MAE = \frac{\sum\lvert Y_{obs} - Y_{pred}\rvert}{n}$	0.0843		Index of errors in the context of predictive modeling studies

The network predicts the data reasonably well, as shown by a graphical depiction that compares predicted values of log I11β-HSD1 with experimentally measured values (Fig. 4). This scatter plot shows a strong positive association. Ten important descriptors were first chosen to be used as input variables in the construction of the ANN model in order to ensure high prediction accuracy and avoid overfitting (Table 4). Additionally, a different test and validation set was used to validate the model. The model's high Q2 value (0.9944) attests to its generalizability. Six of these ten descriptors were examples of 2D topological descriptors, while four of them were 3D geometrical descriptors. This indicates that the biological activity of the chemicals under investigation is significantly influenced by two- and three-dimensional molecular configurations.

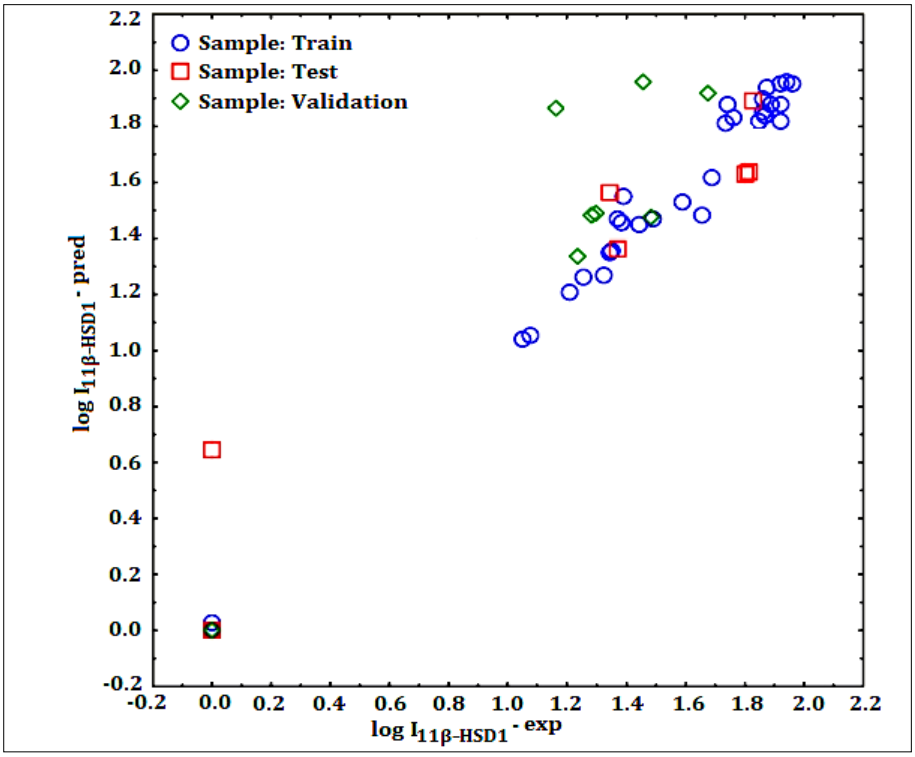

Fig 4: Scatter plot of experimental versus predicted log $I_{11\beta\text{-HSD1}}$ values. Correlation coefficient values: training set R = 0.99; test set R = 0.95; and validation set R = 0.93

The significance of particular descriptors for the 11β-HSD1 inhibitory activity of the examined 2-aminothiazol-4(5H)-one derivatives was demonstrated by the regression analysis utilizing artificial neural network methods and the ensuing sensitivity analysis. The chemical characteristics that most significantly affect the activity of the substances under study were determined by this examination. Table 4 lists the dimensions, block and definition of the descriptors used in the 10-11-1 MLP model in order of significance. Based on error reduction contribution in a sensitivity study, Fig. 5 shows the relative significance of each molecular descriptor in the MLP 10-11-1 model. All of the preselected characteristics were relevant for the MLP 10-11-1 network since every variable that entered the model had an error quotient greater than 1. If a variable had no influence or made the network's performance worse, it would be eliminated.

Table 4: Sensitivity analysis results for the MLP 10-11-1 network

Name	Definition [37]	Category [37]	Dimensionality	Error MLP 10-11-1	Rank
GGI2	Topological charge index of order 2 topological	Galvez topological charge indices (GALVEZ)	2D	16.81	1
MATS1s	Moran autocorrelation of lag 1 weighted by I-state	2D autocorrelations	2D	14.70	2
SpPosA_B(m)	Normalized spectral positive sum from the Burden matrix, weighted by mass	2D matrixbased descriptors	2D	13.18	3
R3v+	R maximal autocorrelation of lag 3/weighted by van der Waals volume	GETAWAY descriptors	3D	10.43	4
R2s	R autocorrelation of lag 2/ weighted by I-state	GETAWAY descriptors	3D	10.12	5
VE1_D/Dt	The coefficient sum of the last eigenvector from the distance/detour matrix	2D matrixbased descriptors	2D	9.40	6
SpMin8_Bh(m)	Smallest eigenvalue n. 8 of the Burden matrix, weighted by mass	Burden eigenvalues	2D	8.70	7
Mor05u	Signal 05/unweighted	3D-MoRSE descriptors	3D	7.98	8
RDF030u	Radial Distribution Function-030/unweighted	RDF descriptors	3D	7.93	9
VE2_B(p)	The average coefficient of the last eigenvector from the Burden matrix, weighted by polarizability	2D matrixbased descriptors	2D	7.86	10

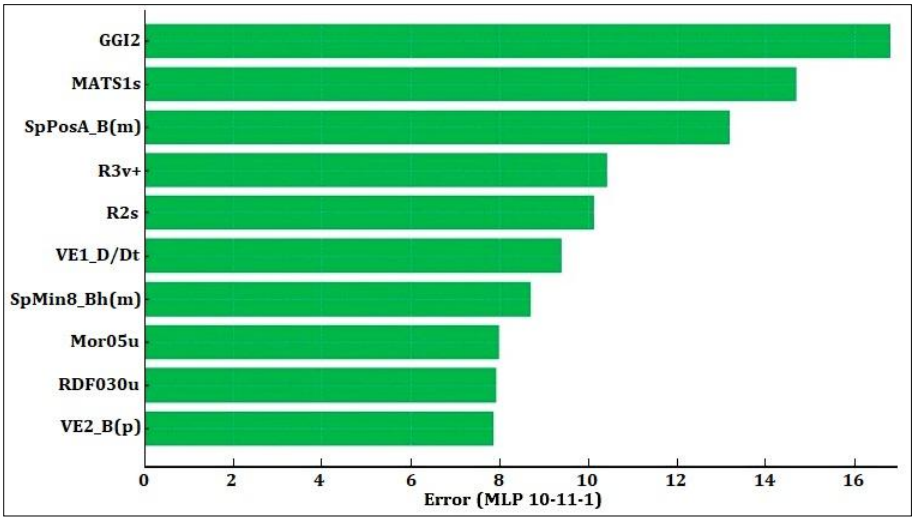

Fig 4: Sensitivity analysis: feature importance of the top 10 descriptors

The presence of large hydrophobic groups (adamantyl and cyclopentyl) in the 5-position of the thiazole ring positively affects the 11β-HSD1 inhibitory activity of compounds containing a pseudothiohydantoin scaffold, according to a number of earlier studies on the search for selective 11β-hydroxysteroid dehydrogenase type 1 inhibitors [18–23]. Specifically, the adamantyl group is known to enhance the drug-like properties of a lead molecule without increasing its toxicity by positively influencing the therapeutic index of many experimental compounds. 39 new candidate inhibitors for 11β-hydroxysteroid dehydrogenase type 1 have been designed after careful consideration of the aforementioned facts and the QSAR model used in the current work. The substantial contribution of 3D descriptors like RDF030u and GETAWAY indices (Table 4), which indicate favorable steric and shape complementarity with the enzyme's binding site, justified the addition of bulky hydrophobic groups like cyclohexyl and tetrahydropyran-methyl moieties. These inhibitors are based on a pseudothiohydantoin scaffold that has cyclohexyl, 2-(tetrahydrofuran-2-yl)methyl, 2-(tetrahydro-2H-pyran-2-yl)methyl, cyclopropyl residues replaced at the amino group, and different substituents at C-5 of the thiazole ring described in Table 5.

Table 5: Designed 2-aminothiazol-4(5H)-one derivatives with 11β-HSD1 inhibitory activity predicted by the MLP 10-11-1 model

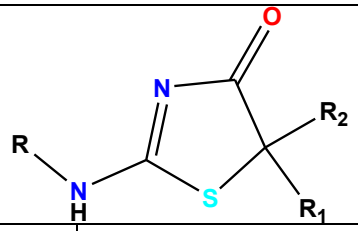

Compound	R	R_1	R_2	Predicted log $I_{11β\text{-}HSD1}$
7b	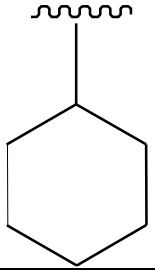	H	CH_3	1.3214
7c		H	C_2H_5	1.3654
7d		H	*n*-C_3H_7	1.9376
7e		H	$CH(CH_3)_2$	1.9213
7f		CH_3	CH_3	1.9128
7g		H	C_6H_5	1.8244
7h		H	*p*-BrC_6H_4	1.3436
7i		C_5H_{10cycl}		2.0133
7j		C_3H_{6cycl}		1.9882
8a		H	H	0.0000
8b		H	CH3	0.9940
8c		H	C2H5	1.0459
8d		H	*n*-C3H7	1.2294

8e	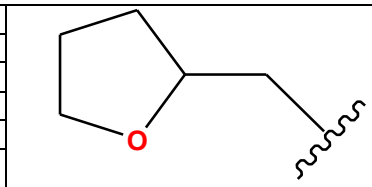	H	CH(CH3)2	1.8577
8f		CH_3	CH_3	1.9598
8g		H	C_6H_5	1.1073
8h		H	*p*-BrC_6H_4	1.8062
8i		C_5H_{10cycl}		1.9745
8j		C_3H_{6cycl}		1.2989
9a	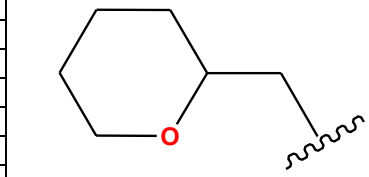	H	H	0.0000
9b		H	CH_3	1.2529
9c		H	C_2H_5	1.2989
9d		H	*n*-C_3H_7	1.4561
9e		H	$CH(CH_3)_2$	1.4561
9f		CH_3	CH_3	2.0031
9g		H	C_6H_5	1.3518
9h		H	*p*-BrC_6H_4	1.9668
9i		C_5H_{10cycl}		2.0226
9j		C_3H_{6cycl}		1.9816
10a	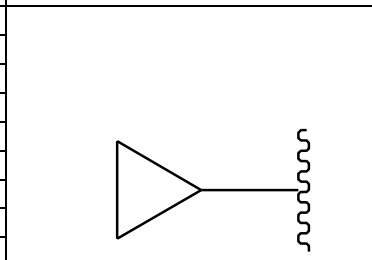	H	H	0.0000
10b		H	CH_3	0.9889
10c		H	C_2H_5	1.0366
10d		H	*n*-C_3H_7	1.1541
10e		H	$CH(CH_3)_2$	1.1541
10f		CH_3	CH_3	0.9889
10g		H	C_6H_5	0.7169
10h		H	*p*-BrC_6H_4	0.6904
10i		C_5H_{10cycl}		1.8769
10j		C_3H_{6cycl}		1.7425

The results indicate that the most promising 11β-hydroxysteroid dehydrogenase type 1 inhibitors may be produced by 2-aminothiazol-4(5H)-one derivatives with cyclohexyl and 2-(tetrahydro-2H-pyran-2-yl)methyl moiety replaced at the amino group. The most active compounds among all developed analogs are 7d, 7e, 7f, 7i, 7j, 8f, 8i, 9f, 9h, 9i and 9j. At a dosage of 10 µM, these compounds may likely decrease isoform 1's activity by more than 80.00%.

In medical chemistry research and drug creation, the pseudothiohydantoin scaffold is crucial and useful. Several substituents have been used to create a variety of compounds having a 2-aminothiazol-4(5H)-one core. Furthermore, as previously noted, scientific literature has described a number of medicinal qualities, such as 11β-hydroxysteroid dehydrogenase type 1 inhibitory activity.

The current study used artificial neural networks to develop a verified QSAR model. Regression difficulties between chemical structure and 11β-HSD1 inhibitory activity of derivatives of 2-aminothiazol-4(5H)-one are solved by this model. It has made it easier to create new compounds and has been used to forecast the inhibitory activity of newly created compounds against 11β-HSD1 (Table 5). In order to avoid overtraining and determine the most important molecular characteristics that influence the 11β-HSD1 inhibitory activity of the pseudothiohydantoin-based compounds under investigation, the MLP 10-11-1 model incorporates ten of the most informative descriptors chosen from a sizable dataset (Tables 1 and 4). Descriptors pertaining to atomic characteristics, including intrinsic state, atomic mass, polarizability, and four unweighted ones, had a substantial impact on the inhibitory action towards 11β-hydroxysteroid dehydrogenase type 1 based on the preselection procedure. These indices, which include both 2D and 3D information from the molecular structure, imply that the model has a respectable degree of predictability since several molecular dimensions affect the modeling activity.

Seven distinct types of descriptors GALVEZ, 2D autocorrelations, 2D matrix-based descriptors, GETAWAY descriptors, Burden eigenvalues, 3D-MoRSE descriptors and RDF descriptors were used to model the 11β-HSD1 inhibitory action of the investigated analogues. According to the sensitivity analysis done (Table 4), the first three descriptors describe the two-dimensional structure of the molecules examined and contribute most to the QSAR model. While MATS1s integrates structural and electronic characteristics, the top-ranked descriptor GGI2 relates to electronic charge distribution, a crucial component in enzyme binding. These results are consistent with earlier studies that highlight the involvement of molecular topology and electrostatics in 11β-HSD1 inhibition [38-40].

The topological charge index of order two, or GGI2, is ranked highest in the sensitivity analysis. The first 10 eigenvalues of the adjusted adjacency matrix of compounds are used to create the Galvez topological charge indices [41, 42]. The topological charge index of order n, where "n" is the order of eigenvalue, is connected to the GGIn descriptors. Molecule charge transfer computed from the adjacency topological matrix is evaluated by the GGI2 descriptor.

The MATS1s descriptor in the aforementioned model belongs to the Dragon descriptors group of 2D autocorrelations [38]. Its

foundation is the autocorrelation of Moran's topological structure. In order to calculate this descriptor, distinct autocorrelation vectors for the lengths of the structural fragments are obtained by adding separate autocorrelation functions for different fragment lengths [39]. An intrinsic state is also utilized as a weighting factor based on a physicochemical feature when computing this descriptor. As a result, MATS1s deals with the topology of the structure or its components in relation to the intrinsic state of the molecules under study.

The third participant descriptor, SpPosA_B(m), is weighted by atomic mass and obtained from the Burden matrix, which is produced from the adjacency matrix [43]. An essential tool for computing molecular descriptors is the adjacency matrix, sometimes referred to as the vertex adjacency matrix [44]. The complete collection of connections between neighboring pairs of atoms is represented by this fundamental graph theoretical matrix. The branching information provided by the adjacency matrix may also be useful for simulating pharmacological activity.

The GETAWAY (Geometry, Topology and Atom-Weights Assembly) descriptors comprise the fourth and fifth indices in the ranking list about relevance to the constructed model. The R3v+ and R2s descriptors make reference to chemical data, atom-relatedness, and three-dimensional molecular geometry. Spatial autocorrelation formulas, connection indices, and conventional matrix operations are used to calculate these descriptors [45]. Their calculation entails examining each atom in the molecule to determine its intrinsic state and atomic van der Waals volume, respectively. According to earlier research, GETAWAY descriptors are a useful tool for creating trustworthy models since they can capture both local and distributed information about the molecule structure [46]. When the property being modeled specifically depends on the 3D aspects of the molecule, as in the case of biological activities, it has been found that using GETAWAY in conjunction with descriptors that contain information on the entire molecular structure appears to create more accurate models. Nevertheless, GETAWAY and topological descriptors yield the most dependable regressions, as in this study [47], even if all molecular descriptor sets successfully model the octanol–water partition coefficient.

The class of 2D matrix-based descriptors includes the previously mentioned descriptor SpPosA_B(m) as well as descriptors VE1_D/Dt and VE2_B(p), which are ranked sixth and last, respectively. The sum of the coefficients in the final eigenvector formed from the distance/detour matrix is represented by VE1-D/Dt. It is computed as the distance from the shortest represents substructure information and is the longest path between vertices from the branching or cyclicity vertices concerning the sections on cations [40]. The total of the coefficients of the final eigenvector, weighted by polarizability, makes up the VE2_B(p). As the number of network vertices increases, so does the value of VE2_B(p) [48].

SpMin8_Bh(m), the eighth important molecular descriptor, falls within the category of burden eigenvalues. Molecular graphs with hydrogen atoms are used to calculate this index using the Burden matrix [49]. The first eight biggest positive eigenvalues of each matrix in the Dragon calculation are often represented as SpMaxk_Bh(w), while the first eight smallest negative eigenvalues are represented as SpMink_Bh(w). Here, k stands for the eigenvalue rank, and w denotes an atomic property, such as atomic mass (m), intrinsic state (s), or polarizability (p), as demonstrated in the instance of SpMin8_Bh(m). The problem of determining the molecular structural similarity or variety of investigated substances can be solved by using this specific molecular descriptor, which takes molecular mass into account.

Another important index included in MoRSE descriptors, or Molecular Representation of Structures based on Electron Diffraction, is Mor05u. The unweighted signal 05 is represented by it. Using a molecular transform generated from an equation used in electron diffraction research, 3D-MoRSE descriptors provide information about compounds based on their three-dimensional structure. These descriptors can accurately encode extremely flexible representations of a compound and reflect the three-dimensional arrangement of atoms within a molecule by taking into account a variety of atomic attributes [40].

The final descriptor in the Radial Distribution Function (RDF) category is RDF030u (Radial Distribution Function 3.0/unweighted). These indices determine the probability that an atom will exist inside a spherical volume with a radius of R. Radial basis functions centered on different interatomic distances ranging from 0.5 to 15.5 Å are used to calculate RDF descriptors, which take into account the amount, characteristics, and distances between atoms. The chemical structure within a 3.0 Å atomic radius of the mass center affects the RDF030u descriptor. As a result, it describes the probability that atoms will be dispersed across a spherical region with the radius stated above. When examining a compound's chemical characteristics, this could be an important factor to take into account [50, 51].

The absence of experimental confirmation of the anticipated inhibitory actions is one of the study's limitations. Furthermore, the model's generalizability to larger chemical spaces may be constrained by the dataset's short size and congeneric series. Our capacity to evaluate the model's performance on unseen chemotypes is limited by the lack of external validation or future forecasts. Additionally, dependence using in silico descriptors without incorporating pharmacokinetic profiling diminishes the suggested candidates. These drawbacks emphasize how crucial it is to conduct more experiments and validate results using structurally different analogs. The most promising class of anticipated molecules, namely pseudothiohydantoin compounds with cyclohexyl and 2-(tetrahydro-2H-pyran-2-yl)methyl residues replaced at the amino group, will be synthesized and biologically evaluated in future studies.

4. CONCLUSIONS

In the current study, a mathematical model for predicting the 11β-hydroxysteroid dehydrogenase type 1 inhibitory activity of fifty-six 2-aminothiazol-4(5H)-one derivatives was developed utilizing QSAR analysis and the ANN algorithm. These compounds have recently been produced and their *in vitro*

activity assessed. Based on its predicted accuracy, the predictive MLP 10-11-1 model was selected from a pool of 500 training networks. Ten molecular descriptors that represent the 2D (topological) and 3D (spatial) characteristics of the compounds under investigation are included in the QSAR model. The findings demonstrated that the main factors influencing the activity of the compounds under investigation were molecular conformation and shape, electrostatic characteristics, intrinsic state, molecular mass, and polarizability.

Additionally, the structural data acquired aided in the creation of novel molecules. The deployment of the developed model to forecast the 11β-HSD1 inhibitory activity of four series of freshly designed analogs was made possible by the validation method, which verified the satisfactory predictive performance. Pseudothiohydantoin compounds with cyclohexyl and 2-(tetrahydro-2H-pyran-2-yl) methyl residues substituted at the amino group, as well as different substituents at C-5 of the thiazole ring, may be viable candidates for future chemical synthesis and biological evaluation, according to the predictions' results. This could also provide more details about the intended biological activity for upcoming in silico research. The results of this investigation may help determine 11β-HSD1 inhibitory activity and develop medications based on the pseudothiohydantoin scaffold for metabolic illnesses. However, in order to properly evaluate the model's generalizability, future experimental validation and application to a wider range of chemical scaffolds are necessary, as the results provided here are based on a very limited and generic dataset.

CONFLICT OF INTEREST

The authors declare no competing interests.

REFERENCES

1. Wami M, Seckl J. Inhibition of 11ß-hydroxysteroid dehydrogenase type 1 as a promising therapeutic target. Drug Discovery Today. 2007;12:504–520.
2. Wang M. Inhibitors of 11β-hydroxysteroid dehydrogenase type 1 in antidiabetic therapy. 2011. p.127–146.
3. Chapman K, Holmes M, Seckl J. 11β-hydroxysteroid dehydrogenases: intracellular gate-keepers of tissue glucocorticoid action. Physiological Reviews. 2013;93:1139–1206.
4. Praveenkumar E, Gurrapu N, Kolluri PK, Yerragunta V, Kunduru BR, Subhashini NJP. Synthesis, anti-diabetic evaluation and molecular docking studies of 4-(1-aryl-1H-1,2,3-triazol-4-yl)-1,4-dihydropyridine derivatives as novel 11β-HSD1 inhibitors. Bioorganic Chemistry. 2019;90:103056.
5. Winnick JJ, Ramnanan CJ, Saraswathi V, Roop J, Scott M, Jacobson P, *et al*. Effects of 11β-hydroxysteroid dehydrogenase-1 inhibition on hepatic glycogenolysis and gluconeogenesis. American Journal of Physiology – Endocrinology and Metabolism. 2013;304:E747–E756.
6. Zhang R, Kan JB, Lu S, Tong P, Yang J, Xi L, *et al*. S100A16-induced adipogenesis is associated with up-regulation of 11β-hydroxysteroid dehydrogenase type 1 (11β-HSD1). Bioscience Reports. 2019. https://doi.org/10.1042/BSR20182042
7. Saklayen MG. The global epidemic of the metabolic syndrome. Current Hypertension Reports. 2018;20:12.
8. Shao S, Zhang X, Zhang M. Inhibition of 11β-hydroxysteroid dehydrogenase type 1 ameliorates obesity-related insulin resistance. Biochemical and Biophysical Research Communications. 2016;478:474–480.
9. Masuzaki H, Paterson J, Shinyama H, Morton NM, Mullins JJ, Seckl JR, *et al*. A transgenic model of visceral obesity and the metabolic syndrome. Science. 2001;294:2166–2170.
10. Peckett AJ, Wright DC, Riddell MC. The effects of glucocorticoids on adipose tissue lipid metabolism. Metabolism. 2011;60:1500–1510.
11. Chapagain A, Caton PW, Kieswich J, *et al*. Elevated hepatic 11β-hydroxysteroid dehydrogenase type 1 induces insulin resistance in uremia. Proceedings of the National Academy of Sciences of the United States of America. 2014;111:3817–3822.
12. Baudrand R, Carvajal CA, Riquelme A, *et al*. Overexpression of 11β-hydroxysteroid dehydrogenase type 1 in hepatic and visceral adipose tissue is associated with metabolic disorders in morbidly obese patients. Obesity Surgery. 2010;20:77–83.
13. Paterson JM, Morton NM, Fievet C, Kenyon CJ, Holmes MC, Staels B, *et al*. Metabolic syndrome without obesity: Hepatic overexpression of 11β-hydroxysteroid dehydrogenase type 1 in transgenic mice. Proceedings of the National Academy of Sciences of the United States of America. 2004;101:7088–7093.
14. Böhme T, Engel CK, Farjot G, Güssregen S, Haack T, Tschank G, *et al*. 1,1-Dioxo-5,6-dihydro-[4,1,2]oxathiazines, a novel class of 11β-HSD1 inhibitors for the treatment of diabetes. Bioorganic & Medicinal Chemistry Letters. 2013;23:4685–4691.
15. Courtney R, Stewart PM, Toh M, Ndongo M-N, Calle RA, Hirshberg B. Modulation of 11β-hydroxysteroid dehydrogenase activity biomarkers and pharmacokinetics of PF-00915275, a selective 11βHSD1 inhibitor. Journal of Clinical Endocrinology & Metabolism. 2008;93:550–556.
16. Joharapurkar A, Dhanesha N, Shah G, Kharul R, Jain M. 11β-hydroxysteroid dehydrogenase type 1: potential therapeutic target for metabolic syndrome. Pharmacological Reports. 2012;64:1055–1065.
17. Gao Q, Kimura RE, Zhang X, Nam J, Amore BM, Hickman D, *et al*. Intestinal and hepatic first-pass extraction of the 11β-HSD1 inhibitor AMG 221 in rats with chronic vascular catheters. Xenobiotica. 2014;44:264–269.
18. Studzińska R, Kołodziejska R, Kupczyk D, Płaziński W, Kosmalski T. Novel derivatives of thiazol-4(5H)-one and their activity in inhibition of 11β-hydroxysteroid

dehydrogenase type 1. Bioorganic Chemistry. 2018;79:115–121.
19. Studzińska R, Kołodziejska R, Płaziński W, Kupczyk D, Kosmalski T, Jasieniecka K, *et al*. Synthesis of N-methyl derivatives of 2-aminothiazol-4(5H)-one and their interactions with 11βHSD1. Chemistry & Biodiversity. 2019. https://doi.org/10.1002/cbdv.201900065
20. Kupczyk D, Studzińska R, Bilski R, Baumgart S, Kołodziejska R, Woźniak A. Synthesis of novel 2-(isopropylamino)thiazol-4(5H)-one derivatives and their inhibitory activity of 11β-HSD1 and 11β-HSD2. Molecules. 2020;25:4233.
21. Kupczyk D, Studzińska R, Baumgart S, Bilski R, Kosmalski T, Kołodziejska R, *et al*. Novel N-tert-butyl derivatives of pseudothiohydantoin as potential anti-cancer targets. Molecules. 2021;26:1–12.
22. Studzi R, Kupczyk D, Wojciech P, Baumgart S, Bilski R, Paprocka R, *et al*. Novel 2-(adamantan-1-ylamino)thiazol-4(5H)-one derivatives and their inhibitory activity toward 11β-HSD1. International Journal of Molecular Sciences. 2021;4:1–17.
23. Baumgart S, Kupczyk D, Archała A, Koszła O, Sołek P, Płaziński W, *et al*. Synthesis of novel 2-(cyclopentylamino)thiazol-4(5H)-one derivatives with potential anti-cancer, antioxidant, and 11β-HSD inhibitory activities. International Journal of Molecular Sciences. 2023;24:1–17.
24. Frisch MJ, Trucks GW, Schlegel HB, *et al*. Gaussian 16, Revision C.01. Gaussian, Inc.; 2016.
25. Dennington R, Keith TA, Millam JM. GaussView, Version 6. Semichem Inc.; 2016.
26. Lee C, Yang W, Parr RG. Development of the Colle–Salvetti correlation-energy formula into a functional of electron density. Physical Review B. 1988;37:785–789.
27. Becke AD. Density-functional exchange-energy approximation with correct asymptotic behavior. Physical Review A. 1988;38:3098–3100.
28. Becke AD. Density-functional thermochemistry. I. Effect of the exchange-only gradient correction. Journal of Chemical Physics. 1992;96:2155–2160.
29. Becke AD. Density-functional thermochemistry. II. Effect of the Perdew–Wang generalized-gradient correlation correction. Journal of Chemical Physics. 1992;97:9173–9177.
30. Becke AD. A new mixing of Hartree–Fock and local density-functional theories. Journal of Chemical Physics. 1993;98:1372–1377.
31. Dragon 7 software. 2017. https://chm.kode-solutions.net/
32. Mauri A, Consonni V, Pavan M, Todeschini R. DRAGON software: An easy approach to molecular descriptor calculations. MATCH Communications in Mathematical and in Computer Chemistry. 2006;56:237–248.
33. Dobchev D, Karelson M. Have artificial neural networks met expectations in drug discovery within QSAR framework? Expert Opinion on Drug Discovery. 2016;11:627–639.
34. TIBCO Statistica User's Guide: Automated Neural Networks Overview. https://docs.tibco.com/pub/stat/14.0.0/doc/html/UsersGuide/GUID-F60C241F-CD88-4714-A8C8-1F28473C52EE.html
35. Roy K, Ambure P, Kar S, Ojha PK. Is it possible to improve the quality of predictions from an "intelligent" use of multiple QSAR/QSPR/QSTR models? Journal of Chemometrics. 2018;32:1–18.
36. Gackowski M, Pluskota R, Koba M. Predicting antitumor activity of anthrapyrazole derivatives using advanced machine learning techniques. Current Computer-Aided Drug Design. 2023. Available from: https://doi.org/10.2174/1573409919666230612144407
37. List of molecular descriptors calculated by Dragon. Available from: http://www.talete.mi.it/products/dragonmoleculardescriptorlist.pdf
38. Singh P, Kumar R, Sharma BK, Prabhakar YS. Topological descriptors in modeling malonyl coenzyme A decarboxylase inhibitory activity: N-alkyl-N-(1,1,1,3,3,3-hexafluoro-2-hydroxypropylphenyl) amide derivatives. Journal of Enzyme Inhibition and Medicinal Chemistry. 2009;24:77–85.
39. Broto P, Moreau G, Vandycke C. Molecular structures: perception, autocorrelation descriptor and SAR studies. European Journal of Medicinal Chemistry. 1984;19:66–70.
40. Ma S, Lv M, Zhang X, Zhai H, Lv W. Computational study of the effects of cations and anions to the cytotoxicity of diverse ionic liquids by supervised machine learning. Chemometrics and Intelligent Laboratory Systems. 2015;144:138–147.
41. Gálvez J, Garcia R, Salabert MT, Soler R. Charge indexes: new topological descriptors. Journal of Chemical Information and Computer Sciences. 1994;34:520–525.
42. Prabhakar Y, Rawal R, Gupta M, Solomon V, Katti S. Topological descriptors in modeling the HIV inhibitory activity of 2-aryl-3-pyridyl-thiazolidin-4-ones. Combinatorial Chemistry & High Throughput Screening. 2005;8:431–437.
43. Todeschini R, Consonni V. Handbook of Molecular Descriptors. Weinheim: Wiley-VCH; 2000.
44. Mansouri K, Ringsted T, Ballabio D, Todeschini R, Consonni V. Quantitative structure–activity relationship models for ready biodegradability of chemicals. Journal of Chemical Information and Modeling. 2013;53:867–878.
45. Ahmed L, Rasulev B, Turabekova M, Leszczynska D, Leszczynski J. Receptor- and ligand-based study of fullerene analogues: comprehensive computational approach including quantum-chemical, QSAR and molecular docking simulations. Organic & Biomolecular Chemistry. 2013;11:5798–5808.

46. Al-Fakih AM, Aziz M, Abdallah H, Maarof H, Jamaludin R, Usman B. Corrosion inhibition of Q235a steel in acid medium using isatin derivatives: a QSAR study. Malaysian Journal of Analytical Sciences. 2016;20:484–490.
47. Consonni V, Todeschini R, Pavan M, Gramatica P. Structure/response correlations and similarity/diversity analysis by GETAWAY descriptors. 2. Application of novel 3D molecular descriptors to QSAR/QSPR studies. Journal of Chemical Information and Computer Sciences. 2002;42:693–705.
48. Costa AS, Martins JPA, de Melo EB. SMILES-based 2D-QSAR and similarity search for identification of potential new scaffolds for development of SARS-CoV-2 Mpro inhibitors. Structural Chemistry. 2022;33:1691–1706.
49. Yu X. Prediction of depuration rate constants for polychlorinated biphenyl congeners. ACS Omega. 2019;4:15615–15620.
50. De Melo EB, Moura E Silva S, Paula FR. Molecular modelling and quantitative structure–activity relationship studies of anatoxin-a and epibatidine derivatives with affinity to rodent nAChR receptors. Chemical Papers. 2014;68:1121–1131.
51. Dinparast L, Dastmalchi S. A QSAR study on the 4-substituted coumarins as potent tubulin polymerization inhibitors. Advanced Pharmaceutical Bulletin. 2020;10:271–277.

About the Corresponding Author
Ashok Nagore is affiliated with the Department of Chemistry at PMCOE, Government Science College, Rewa, Madhya Pradesh, India. He is engaged in teaching and research in chemical sciences, with a focus on academic excellence, student development, and contributing to scientific knowledge through scholarly activities and institutional involvement.